Charge Recombination in Dye-Sensitized Nanocrystalline TiO_2 Solar Cells

S. Y. Huang,[†] G. Schlichthörl,[†] A. J. Nozik,[†] M. Grätzel,[‡] and A. J. Frank*,[†]

National Renewable Energy Laboratory, Golden, Colorado 80401, and Institut de Chimie Physique, Ecole Polytechnique Fédérale, CH-1015 Lausanne, Switzerland

Received: August 6, 1996; In Final Form: November 1, 1996[⊗]

Charge recombination between dye-sensitized nanocrystalline TiO_2 electrodes and the I_3^-/I^- couple in nonaqueous solution is described. The sensitizer was $[RuL_2(NCS)_2]$ (L = 2,2′-bipyridyl-4,4′-dicarboxylic acid). An apparent inequality between the dark current and the recombination current is ascribed to a voltage shift caused by a potential drop at the SnO_2/TiO_2 interface, ohmic losses in the SnO_2 and TiO_2, and an overpotential for the redox reaction at the Pt counter electrode. Treating the dye-coated TiO_2 electrodes with pyridine derivatives (4-*tert*-butylpyridine, 2-vinylpyridine, or poly(2-vinylpyridine)) improves significantly both the open-circuit photovoltage V_{oc} (from 0.57 to 0.73 V) and the cell conversion efficiency (from 5.8 to 7.5%) at a radiant power of 100 mW/cm^2 (AM 1.5) with respect to the untreated electrode. An analytical expression relating V_{oc} to the interfacial recombination kinetics is derived, and its limitations are discussed. Analysis of V_{oc} vs radiant power data with this expression indicates that the pyridine compounds may lower the back-electron-transfer rate constant by 1−2 orders of magnitude. The pyridines are found to have no significant effect on the recombination mechanism and kinetics of electron injection from excited dye molecules to TiO_2. Studies of the dye-covered electrodes show that the rate of recombination is second order in I_3^- concentration, which is attributed to the dismutation reaction $2I_2^- \rightarrow I_3^- + I^-$ with I_2 as the electron acceptor in the back-reaction. Mass-transport theory is applied to understand the dependence of the short-circuit photocurrent on the radiant power at low I_3^- concentration and to calculate the diffusion coefficient of I_3^- ions (7.6×10^{-6} cm^2/s) in the porous TiO_2 structure. The dependence of other cell parameters on the I_3^- concentration is also investigated.

Introduction

Dye-sensitized photochemical solar cell systems based on highly porous nanocrystalline films of titanium dioxide are of considerable technological interest because of their demonstrated high-power conversion efficiency (7−10% at AM 1.5),[1−18] potential low cost,[19] and high semiconductor stability. The most extensively studied cell (Figure 1a) consists of a monolayer of a Ru−bipyridyl-based charge-transfer dye adsorbed onto the surface of a thin nanocrystalline TiO_2 film (ca. 10 μm) supported on transparent SnO_2 conducting glass. The particles of the film are in contact with an electrolyte solution containing iodide and triiodide ions as a redox relay and are sandwiched by a second plate of electrically conducting glass covered with platinum. Figure 1b illustrates the general mechanism of photosensitization. Photocurrent is generated when visible light absorption by the dye leads to electron injection into the conduction band of TiO_2. The injected electrons diffuse through the interconnecting network of TiO_2 particles and are collected at the transparent conducting electrode. The resulting oxidized dye molecules are reduced by I^- ions, regenerating the original dye molecule. The oxidized iodide ions diffuse back to the Pt counter electrode as I_3^- ions, where reduction occurs to complete the cyclic process.

A major factor limiting the conversion efficiency of present dye-sensitized TiO_2 solar cells is the low photovoltage,[20] which is substantially below the theoretical maximum.[21−23] Charge recombination at the nanocrystallite/redox electrolyte interface is expected to play a significant role in lowering the photovoltage. There are two likely recombination pathways, occurring at the interface. The injected conduction-band electrons may recombine with oxidized dye molecules or react with redox species in the electrolyte. Owing to the rapid rate of reduction of the ionized dye molecules by I^- ions, which are present at high concentration, the contribution of this energy-loss channel to the recombination current can usually be ignored.[24,25] The net recombination process, controlling the photovoltage, is represented by the reaction[7]

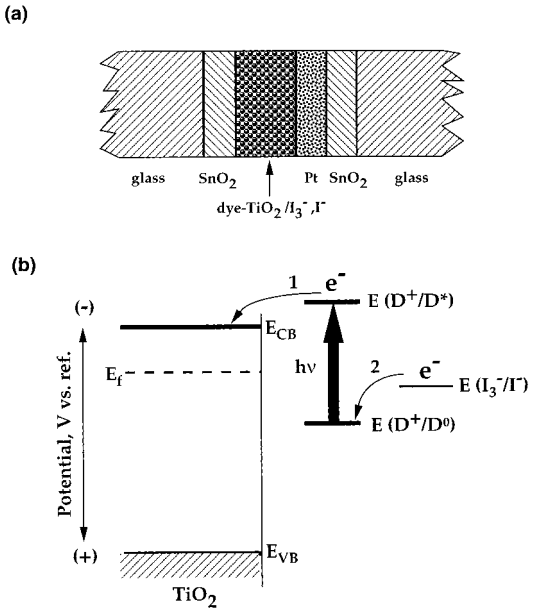

Figure 1. (a) Schematic of a dye-sensitized nanocrystalline TiO_2 solar cell. (b) Energy level diagram for dye sensitization of n-TiO_2: (1) charge injection from excited state of dye to conduction band of TiO_2 and (2) reduction of the oxidized dye by I^- ions to regenerate the original dye.

[†] National Renewable Energy Laboratory.
[‡] Ecole Polytechnique Fédérale.
[⊗] Abstract published in *Advance ACS Abstracts,* March 1, 1997.

S1089-5647(96)02377-2 CCC: $14.00

$$2e^- + I_3^- \rightarrow 3I^- \quad (1)$$

The back electron transfer (eq 1) can, in principle, take place at the surface of not only TiO_2 but also SnO_2 because of the porous nature of the TiO_2 film. It is reported,[20] however, that the reaction occurs almost entirely at the TiO_2 particle/redox electrolyte solution interface as a result of the relatively large surface area of the nanocrystalline film. Some suppression of back electron transfer in TiO_2 and other semiconductor systems, as manifested by a higher open-circuit photovoltage V_{oc}, has been achieved by passivating recombination centers with 4-*tert*-butylpyridine.[7,8,26]

In this article, we report on the effect of various pyridine compounds on the recombination kinetics and cell parameters. An unexpected result is the discovery that the reaction rate for recombination is second order in I_3^- concentration. A quantitative relationship between V_{oc} and the rate constant parameter is derived. The mass-transport theory is also applied to understand the dependence of the short-circuit photocurrent J_{sc} on light intensity at low I_3^- concentration and to determine the diffusion coefficient of I_3^- ions through the nanoporous TiO_2 film.

Theory

Open-Circuit Photovoltage. We consider a dye-sensitized n-type semiconductor in contact with a redox electrolyte. Upon photoexcitation of sensitizing dye molecules (Figure 1), electrons are injected into the conduction band, where they travel through the semiconductor, exit at the rear contact, flow through an external load, and then react with the adsorbed oxidized half of the redox couple at the counter electrode/electrolyte interface. Alternatively, the injected electrons can undergo surface recombination with either the oxidized half of the redox couple in solution or oxidized dye molecules; however, at the high concentration of I^- ions used in this study, recombination of injected electrons with dye molecules can be neglected.[9,24,25] The observed photocurrent density J_{ph} is thus given by

$$J_{ph} = J_{inj} - J_r \quad (2)$$

where J_{inj} is the electron injection current resulting from dye sensitization and J_r is the surface recombination current. J_{inj} is related to the incident photon flux I_0 (cm^{-2} s^{-1}) by the expression

$$J_{inj} = qAI_0 \quad (3)$$

where q is the electronic charge and A is the ratio of absorbed photon flux to I_0. When the spectral distribution of a light source is independent of the incident radiant power (mW/cm^2) P_0, I_0 is proportional to $P_0 = (kT)^{-1} \int_0^\infty h\nu I(h\nu)\, dh\nu$, where $I(h\nu)$ is the incident photon flux at a specific quantum energy. The recombination current depends on the rate constant for back electron transfer k_{et}, the concentration of the oxidized half of the redox couple c_{ox}, and the difference between the electron population in the semiconductor present in the dark n_0 and in the light n.

$$J_r = qk_{et}c_{ox}^m(n^{u\alpha} - n_0^{u\alpha}) \quad (4)$$

where the order of the rate of reaction is expressed as the exponents m for the oxidized redox species and u for electrons; α is the electron-transfer coefficient. Equation 4 is just a variation of the Butler−Volmer expression for semiconductor electrodes.[27] The electron population n is exponentially related to the photovoltage V by the equation

$$n = n_0 \exp[qV/kT] \quad (5)$$

where $qV = E_f - E_{fo}$; E_f and E_{fo} are the respective Fermi levels of TiO_2 in the light and in the dark.

At open circuit ($V = V_{oc}$), $J_{ph} = 0$, and from eqs 3 and 4, we obtain

$$qAI_0 = qk_{et}c_{ox}^m(n^{u\alpha} - n_0^{u\alpha}) \quad (6)$$

Combining eqs 5 and 6 gives the dependence of V_{oc} on the light intensity, the concentration of oxidized redox species, and the back-electron-transfer rate constant.

$$V_{oc} = \frac{kT}{qu\alpha} \ln\left(\frac{AI_0}{n_0^{u\alpha}k_{et}c_{ox}^m} + 1\right) \quad (7)$$

Usually, $AI_0 \gg n_0^{u\alpha}k_{et}c_{ox}^m$, and eq 7 is simplified as follows:

$$V_{oc} = \frac{kT}{qu\alpha} \ln\left(\frac{AI_0}{n_0^{u\alpha}k_{et}c_{ox}^m}\right) \quad (8)$$

A similar expression has been used to elucidate the dependence of V_{oc} on c_{ox} and k_{et} in regenerative photoelectrochemical systems,[28] including dye-sensitized TiO_2 solar cells,[7] except that the reaction orders and the electron-transfer coefficient were effectively taken as unity.[7,28] It is informative to examine some of the assumptions underpinning the derivation of eq 8. First of all, no distinction between localized electrons in surface states and free electrons in the conduction band is made in eq 4; both may contribute to the recombination current. However, the photovoltage in eq 5 is controlled only by conduction-band electrons. Thus, if part of the total electronic charge, which is determined by both the injection current and recombination kinetics, is trapped in surface states, a lower V_{oc} is expected. Furthermore, unlike conventional solid-state devices, n_0 is not the same as the doping density of the semiconductor. In the dark, the particle film, in contact with the redox electrolyte, is likely depleted of electron—the resulting potential drop, however, is negligible due to the small (nanometer) size of the semiconductivity particles. In particular, n_0 depends on the difference between the conduction band edge E_c and the redox potential of the solution E_{redox} as expressed by $n_0 = N_c \exp[(E_c - E_{redox})/kT]$, where N_c is the effective density of states in conduction band. Thus, a band edge shift in the dark, corresponding to change in n_0, would also affect V_{oc}. For example, a band edge shift may result from the adsorption or desorption of charge species (ions) in the electrolyte solution.

From eq 8, we obtain expressions for $u\alpha$ and m.

$$\frac{dV_{oc}}{d \ln I_0} = \frac{kT}{qu\alpha} \quad (9)$$

$$\frac{dV_{oc}}{d \ln c_{ox}}\left(\frac{dV_{oc}}{d \ln I_0}\right)^{-1} = -m \quad (10)$$

Diffusion-Limited Photocurrent. When the concentration gradient of oxidized species in solution controls the photocurrent

$$J_{ph} = -zFD\frac{dc_{ox}(x)}{dx} \quad (11)$$

where $c_{ox}(x)$ is the concentration of oxidized species in solution at location x between the SnO_2/TiO_2 interface ($x = 0$) and the platinum counter electrode ($x = d$), z is the number of electrons transferred from TiO_2 to an oxidized species, D is the diffusion

coefficient of the oxidized species, and F is the Faraday constant. In the following analysis, we assume that the concentration gradient of oxidized species (I_3^-) is constant. This assumption leads to an overestimation of D. Analysis of this error using a more complete model[29] indicates that the resulting systematic error is well within the experimental uncertainty (<20%) arising from, for example, variations in the thickness and the porosity of TiO_2 films.

For a constant photocurrent, corresponding to a fixed concentration gradient across the cell, we obtain with the aid of eq 11 the relation

$$c_{ox}(x) = B - \frac{J_{ph}}{zFD}x \tag{12}$$

where B is a constant. Assuming that the total amount of oxidized species is invariant, the integral of eq 12 yields

$$\frac{1}{d}\int_0^d c_{ox}(x)\,dx = c_{ox}^0 = B - \frac{J_{ph}}{2zFD}d \tag{13}$$

where c_{ox}^0 is the initial or average concentration of oxidized species in solution. Solving for B, we obtain $B = c_{ox}^0 + (J_{ph}/2zFD)d$, which, when substituted into eq 12, gives

$$c_{ox}(d) = c_{ox}^0 - \frac{J_{ph}}{2zFD}d \tag{14}$$

for $x = d$. Equation 14 gives the limiting value of the short-circuit photocurrent density at high light intensity when $c_{ox}(d)$ goes to zero at the counter electrode: $J_{sc} = 2c_{ox}^0 zFD/d$.

Assuming that changes in the I^- concentration, which is in large excess, can be neglected, the shift of potential ΔV at the Pt cathode with $c_{ox}(d)$ is described by the Nernst equation $\Delta V = (-kT/q)\ln(c_{ox}^0/c_{ox}(d))$, where ΔV is measured with respect to the redox potential of the solution in the dark. Substituting eq 14 into the Nernst expression gives the relation

$$\Delta V = \frac{-kT}{q}\ln\left(\frac{c_{ox}^0}{c_{ox}^0 - \frac{J_{sc}d}{2zFD}}\right) \tag{15}$$

At short circuit ($V = 0$), the potential of the Pt cathode and the TiO_2 film is equal. Thus, concomitant with the shift of the cathode potential with radiant power, the electron concentration in the conduction band changes. From eqs 5 and 15, the dependence of the conduction-band electron concentration on c_{ox}^0 and J_{sc} is obtained.

$$n = n_0\frac{c_{ox}^0}{c_{ox}^0 - \frac{J_{sc}d}{2zFD}} \tag{16}$$

Combining eqs 4 and 16 yields the recombination current at short circuit.

$$J_r = qk_{et}c_{ox}(x)^m n_0^{u\alpha}\left[\left(\frac{c_{ox}^0}{c_{ox}^0 - \frac{J_{sc}d}{2zFD}}\right)^{u\alpha} - 1\right] \tag{17}$$

For a second-order reaction, $m = 2$, and $c_{ox}(x)^2$ is replaced by the average of $c_{ox}(x)^2$ across the cell.

$$J_r = qk_{et}n_0^{u\alpha}\left[\left(\frac{c_{ox}^0}{c_{ox}^0 - \frac{J_{sc}d}{2zFD}}\right)^{u\alpha} - 1\right]\left[(c_{ox}^0)^2 + \frac{1}{3}\left(\frac{J_{sc}d}{2zFD}\right)^2\right] \tag{18}$$

where the last terms in brackets correct for the difference between the average of the square and the square of the average of $c_{ox}(x)$.

Combining eqs 2, 3, and 18, we obtain the dependence of J_{sc} at low c_{ox}^0 on the light intensity (or J_{inj}).

$$qAI_0 = J_{sc} + qk_{et}n_0^{u\alpha}\left[\left(\frac{c_{ox}^0}{c_{ox}^0 - \frac{J_{sc}d}{2zFD}}\right)^{u\alpha} - 1\right]\left[(c_{ox}^0)^2 + \frac{1}{3}\left(\frac{J_{sc}d}{2zFD}\right)^2\right] \tag{19}$$

Experimental Section

cis-Dithiocyanato-*N*,*N*-bis(2,2′-bipyridyl-4,4′-dicarboxylic acid)−ruthenium(II) dihydrate, $[RuL_2(NCS)_2]\cdot 2H_2O$ (Solaronix), TiO_2 colloidal solution (Solaronix), and poly(2-vinylpyridine) (Polysciences; MW 7000, 99%) were used as received. 3-Methyl-2-oxazolidinone, NMO (Aldrich), 4-*tert*-butylpyridine (Aldrich), and 2-vinylpyridine (Aldrich) were vacuum-distilled. Acetonitrile (Aldrich, 99.9%) was dried over CaH_2 and distilled under N_2. Other reagents were obtained from vendors at the highest commercial purity and used as received.

The preparation of nanocrystalline TiO_2 films was adapted from the literature.[7,19] Conducting glass plates (2.5 × 10 cm; Nippon Sheet Glass; F-doped SnO_2 overlayer, 81% transmission in the visible, 2−5% haze, 10 Ω/sq) were used as the substrate for depositing TiO_2 films. To control the thickness of the TiO_2 film and to mask electrical contact strips, 0.5 cm width of the conducting glass plate was covered along the length of each edge with adhesive tape (Scotch), having a nominal thickness of 40 μm. A drop (0.5 μL/cm^2) of 10 mM titanium butoxide in 2-propanol was spread uniformly on the surface of the glass.[19] A viscous TiO_2 colloidal solution was then spread on top of the first layer. After removing the adhesive tapes, the assemblage was heated in air for 30 min at 450 °C and then allowed to cool. The film was then covered with a layer (0.5 mL/cm^2) of 0.3 M $TiCl_4$ in water overnight in a closed chamber filled with air, washed with distilled water, and before exposure to dye solution, annealed again at 450 °C for 30 min. The thickness of the resulting films was about 8 μm as measured with a Tencor Alpha-Step profiler.

The TiO_2 electrodes were coated with the dye by soaking them overnight (≃10 h) in 3×10^{-4} M $[RuL_2(NCS)_2]\cdot 2H_2O$ in absolute ethanol at room temperature and then drying them in a stream of N_2. To minimize rehydration of the TiO_2 surface from moisture in ambient air, which causes the dye to desorb, the electrodes, while still warm (80−100 °C) from annealing, were exposed to the dye solution. The dye-coated nanocrystalline TiO_2 electrodes or undyed TiO_2 powder was soaked in either 4-*tert*-butylpyridine (TBP), 2-vinylpyridine (VP), or 50 mM poly(2-vinylpyridine) (PVP) in CH_3CN for 15 min and then dried under a N_2 stream. Similar precautions against moisture were taken with electrodes undergoing treatment with the pyridine derivatives.

Pt counter electrodes with a mirror finish were prepared by electron beam, depositing a 60 nm layer of Pt on top of a 40 nm layer of Ti on a glass plate. The Pt electrode and the dye-coated TiO_2 electrode were clamped firmly together, and a small quantity of redox electrolyte solution was introduced into the porous structure of the TiO_2 film by capillary action. The dye-

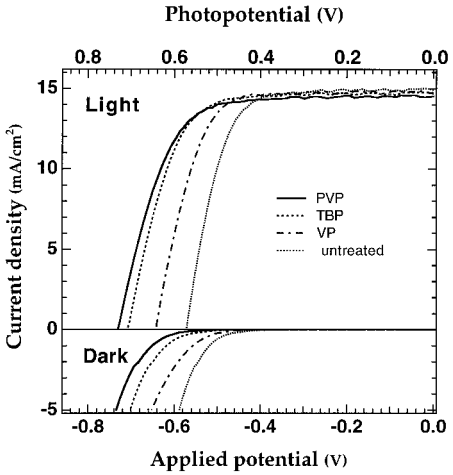

Figure 2. Photocurrent−voltage and dark current−voltage curves of untreated and pyridine derivative-treated $[RuL_2(NCS)_2]$-coated nanocrystalline TiO_2 electrodes in CH_3CN/NMO (50:50 wt %) containing LiI (0.3 M) and I_2 (30 mM). The pyridines include poly(2-vinylpyridine) (PVP), 4-*tert*-butylpyridine (TBP), and 2-vinylpyridine (VP). The radiant power is 100 mW/cm^2 (AM 1.5).

coated TiO_2 film was illuminated through the transparent conducting glass support. An aperture on the sample holder restricted the illumination area of the cell to 0.44 cm^2.

The intensity of the absorption band of I_3^- ions at 362 nm ($\epsilon = 2.3 \times 10^4$ M^{-1} cm^{-1})[30] was used to evaluate the triiodide ion concentration. The UV−vis absorption spectra were measured with a Varian Cary 5E spectrophotometer. (Photo)-current−voltage measurements were performed using a Keithley Model 236 source measure unit. An Oriel 150 W Xe arc lamp, equipped with Oriel 51942 and Oriel AMO optical filters, was used as a light source for simulating the solar spectrum at AM 1.5. The spectral irradiance of the solar simulator (as determined with an IL-COR 1800 spectroradiometer) closely matched that of the standard AM 1.5 solar spectrum[31] over the spectral response of the $[RuL_2(NCS)_2]$-sensitized nanocrystalline TiO_2 electrodes. As an indication of the closeness of the match, the respective theoretical J_{sc} maxima of the solar simulator and the standard AM 1.5 solar spectrum were calculated[32] to be 25 and 27 mA/cm^2 for the spectral region over which the sensitizing dye absorbs (300−800 nm). The incident radiant power was measured before each experiment with a YSI A65 radiometer. The experimental photocurrent density−radiant power data were analyzed using the nonlinear curve-fitting procedure in Kaleidagraph (Synergy Software).

Results and Discussion

Figure 2 displays the current−voltage characteristics of $[RuL_2(NCS)_2]$-coated nanocrystalline TiO_2 electrodes exposed to 4-*tert*-butylpyridine (TBP), 2-vinylpyridine (VP), or poly(2-vinylpyridine) (PVP). The electrodes were immersed in CH_3CN/NMO (50:50 wt %) containing 0.3 M LiI and 30 mM I_2. A comparison of the current of the electrodes at a given potential reveals that the dark current J_d is much smaller than J_r , which is measured as the difference between J_{sc} and J_{ph}. This apparent inequality is ascribed to a shift of potential and can be understood from Figure 3 and the following analysis. In the dark, electrons flow from the SnO_2 film across the SnO_2/TiO_2 interface, the TiO_2/solution interface, and then the solution/Pt interface. In the light, the direction of the electron flux is reversed. For electron transfer to occur, the potential of SnO_2 must be negative of the TiO_2 potential in the dark and positive of it in the light. Correspondingly, the potential of the Pt electrode must be positive of the redox potential in the dark

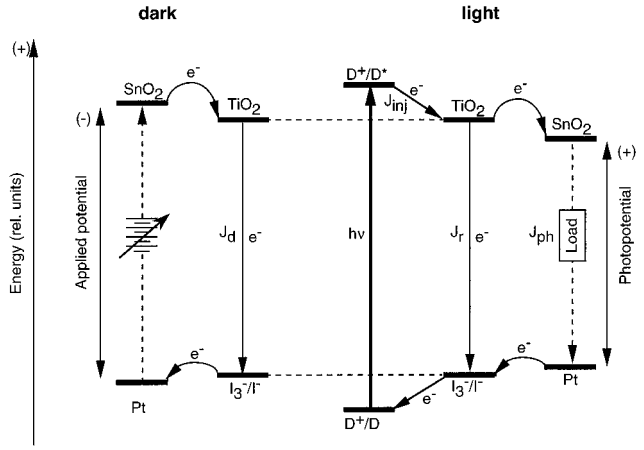

Figure 3. Energy levels and electron transfer pathways for a dye-covered TiO_2 solar cell in the dark and under illumination. Electron transfer from the Fermi level of TiO_2 to the charge mediator I_3^- (eq 1) constitutes both the dark current J_d and the recombination current J_r. When $J_d = d_r$, the TiO_2 potential is fixed, whether the current is a consequence of the (dark) applied bias or the light-induced charge injection J_{inj} from the dye (D^+/D^*). The applied bias between the SnO_2 and Pt electrode depends on ohmic losses within the SnO_2 and TiO_2 (not shown in figure), the potential drop at the SnO_2/TiO_2 interface, and the overpotential for the redox reaction at the Pt electrode. When $J_d = J_r$, the applied potential at the SnO_2 contact is shifted negatively with respect to the photopotential.

and negative of it in the light. Electron injection from TiO_2 to the charge mediator I_3^- constitutes both J_d and J_r. Under the conditions of measurements, the rate of back electron transfer from TiO_2 to the redox species in solution is not limited by mass transport of I_3^- ions. Thus, the redox potential of the solution is not affected by the current and is the same in both the dark and the light. Furthermore, recombination of electrons with oxidized dye molecules is significantly slower than the reduction of the dye by I^- ions.[9,24,25] Thus, the electron concentration in TiO_2 governs both the magnitude of the current and the position of the Fermi level or potential of TiO_2. In other words, when J_d and J_r are the same, the potential of TiO_2 in the dark equals that in the light. On the other hand, the applied bias between the SnO_2 film and the Pt counter electrode depends on ohmic losses within the SnO_2 and TiO_2, a potential drop at the SnO_2/TiO_2 interface because of the presence of a barrier, and the overpotential for the redox reaction at the Pt electrode. Additional bias may be required to offset these potential losses. Thus, to generate the same J_d and J_r, the applied potential at the SnO_2 contact in the dark is shifted negatively with respect to the photopotential. For example, in the case of the PVP-treated dye−TiO_2 system (Figure 2), to produce a dark or recombination current of 4 mA/cm^2 requires a potential of −0.72 and −0.62 V, respectively, corresponding to a −100 mV potential shift for the dark reaction.

Figure 4a shows that J_{sc} of untreated and pyridine derivative-treated $[RuL_2(NCS)_2]$-coated TiO_2/CH_3CN−NMO (50:50 wt %), LiI (0.3 M), I_2 (30 mM)/Pt is essentially the same and varies in direct proportion to the radiant power up to the maximum illumination level studied (14.2 mA/cm^2 at 100 mW/cm^2). The coincidence of the J_{sc} vs radiant power plots imply that $J_{sc} \simeq J_{inj}$ (i.e., $J_r \simeq 0$; eq 3). In other words, the pyridine compounds do not significantly affect the injection current. These conclusions are supported by the observation (Figure 2) that the photocurrent is essentially constant between 0 and −0.4 V. Furthermore, these results are consistent with reports that the quantum yield for charge collection in dye-sensitized TiO_2 particle electrodes is close to unity.[9,10,33]

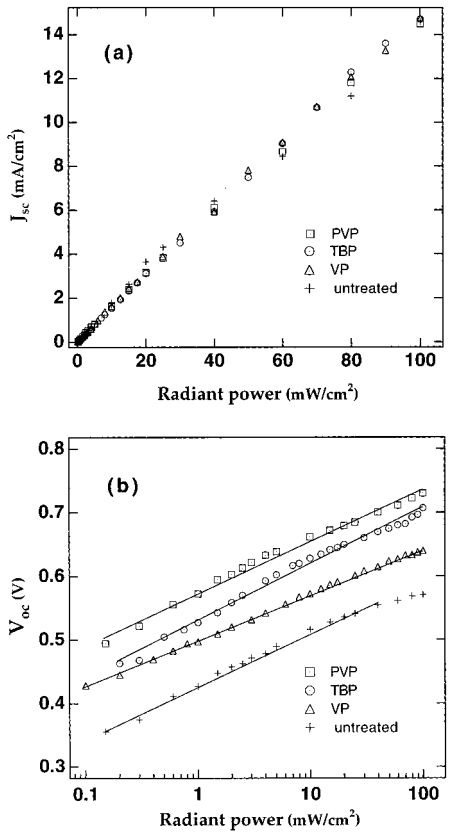

Figure 4. (a) J_{sc} vs radiant power and (b) V_{oc} vs ln(radiant power) plots for untreated and pyridine derivative-treated [$RuL_2(NCS)_2$]-coated nanocrystalline TiO_2 electrodes in CH_3CN/NMO (50:50 wt %) containing LiI (0.3 M) and I_2 (30 mM).

TABLE 1: Photocurrent−Voltage Characteristics of Untreated and Pyridine Derivative-Treated [$RuL_2(NCS)_2$]-Coated Nanocrystalline TiO_2 Solar Cells[a,b]

electrode treatment	J_{sc} (mA/cm^2)	V_{oc} (mV)	FF	η (%)
untreated	14.9	570	0.68	5.8
VP[c]	14.8	640	0.70	6.6
TBP[c]	14.7	710	0.72	7.5
PVP[c]	14.5	730	0.71	7.5

[a] Radiant power: 100 mW/cm^2 (AM 1.5). [b] Redox electrolyte: CH_3CN/NMO (50:50 wt %), LiI (0.3 M), and I_2 (30 mM). [c] VP (2-vinylpyridine); TBP (4-*tert*-butylpyridine); PVP (poly(2-vinylpyridine)).

Figure 4b shows the logarithmic dependence of V_{oc} on the incident radiant power over a range of 0−100 mW/cm^2. For both the untreated and pyridine derivative-treated dye−TiO_2 electrodes, values of the product $u\alpha$, obtained from the slope of the linear portion of the plots and eq 9, are virtually the same ($u\alpha = 0.7$), suggesting that the pyridine derivatives do not significantly alter the mechanism of back electron transfer. On the other hand, it can be seen from Figure 4b or Table 1 that treating $RuL_2(NCS)_2$]−TiO_2 electrodes with pyridine derivatives improves V_{oc}. At a P_0 of 100 mW/cm^2, the improvement of V_{oc} with respect to the untreated surface ($V_{oc} = 0.57$ V) ranges from 0.64 V, for the VP-treated sample, to 0.73 V, for the PVP-treated sample, corresponding to respective increases of 70 and 160 mV. From Table 1 and eq 8, the increase of V_{oc} upon treating the [$RuL_2(CNS)_2$]−TiO_2 surface with VP, TBP, and PVP respectively correlates with an apparent decrease of the back-electron-transfer rate constant of 9-, 26-, and 69-fold with respect to k_{et} of the untreated surface. It is important to point out, however, that eq 8 does not consider the possible role of surface-state charging or conduction-band edge shift. These phenomena can also account for the effect of pyridine derivatives

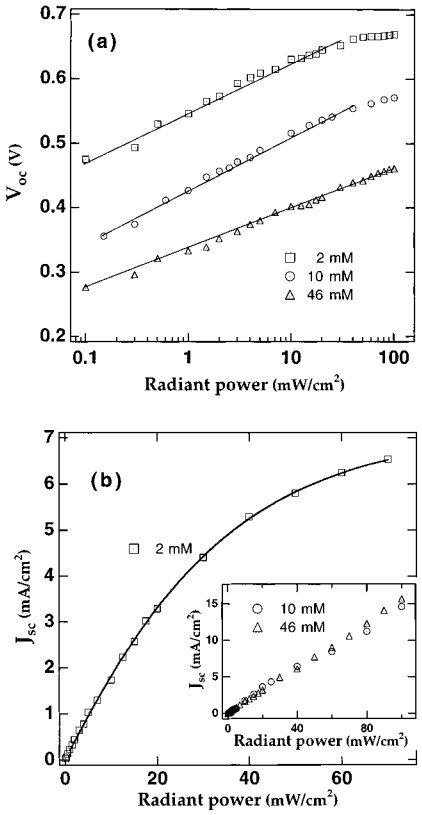

Figure 5. (a) V_{oc} vs ln(radiant power) and (b) J_{sc} vs radiant power plots for untreated [$RuL_2(NCS)_2$]-coated nanocrystalline TiO_2 electrodes in CH_3CN/NMO (50:50 wt %) containing various I_3^- concentrations (2, 10, 46 mM) at a fixed LiI/I_2 concentration ratio (0.06 M/6 mM, 0.3 M/30 mM, and 1.5 M/150 mM, respectively). (b) Experimental data, open squares; theoretical curve, line.

on the observed increase of V_{oc}. The higher V_{oc}, at both a constant J_{sc} and fill factor FF (0.7), increases the cell efficiency from 5.8% (untreated surface) to 7.5% (PVP-treated surface), corresponding to a 29% improvement (Table 1).

Figure 5 shows V_{oc} vs ln P_0 and J_{sc} vs P_0 plots for untreated [$RuL_2(NCS)_2$]-coated TiO_2 electrodes as the I_3^- concentration is varied; the redox potential of I_3^-/I^- was held constant by maintaining the same concentration ratio of LiI/I_2. The value of V_{oc} in Figure 5a depends strongly on the I_3^- concentration. As the I_3^- concentration decreases, V_{oc} increases at all illumination levels. For example, at a radiant power of 100 mW/cm^2, a decrease of the I_3^- concentration from 46 to 2 mM is associated with an increase of V_{oc} from 0.46 to 0.67 V, corresponding to a voltage shift of 210 mV. At high I_3^- concentration (46 mM), V_{oc} varies linearly with ln P_0 up to a radiant power of 100 mW/cm^2, whereas at low I_3— concentration (<10 mM), the plots show a negative deviation from linearity at a radiant power higher than 40 mW/cm^2. An examination of eq 8 suggests that the decrease of V_{oc} may arise from an increase of I_3^- concentration. The additional I_3^- ions is a consequence of accumulated electrons in TiO_2, via charge injection from excited dye molecules, coupled with a decrease of I^- ions during the regeneration of the oxidized dye. A higher V_{oc} implies a larger electron concentration in TiO_2 (eq 5), which, in turn, leads to a higher I_3^- concentration in solution. Thus, an illuminated cell with an initially low I_3^- concentration (i.e., high V_{oc}) will generate a larger amount of I_3^- ions than one with an initially high I_3^- concentration (i.e., low V_{oc}). The additional light-produced I_3^- ions lowers the electron concentration in TiO_2, via the back-reaction, and increases the difference between the measured photovoltage at high radiant power and

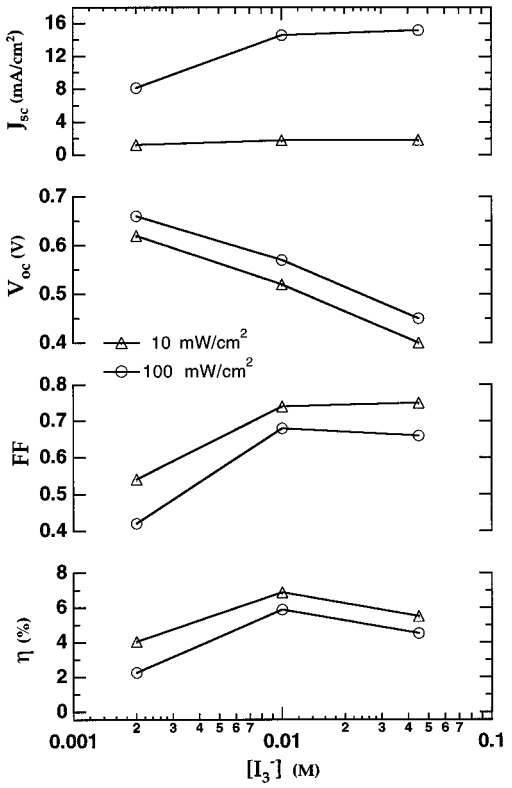

Figure 6. Dependence of J_{sc}, V_{oc}, FF, and η (%) on ln[I_3^-] at different radiant power for untreated [$RuL_2(NCS)_2$]-coated nanocrystalline TiO_2 electrodes in CH_3CN/NMO (50:50 wt %); LiI/I_2 concentration ratio is fixed as described in Figure 5.

that obtained from the linear extrapolation of the V_{oc} vs ln P_0 plot determined at low radiant power.

Figure 6 shows the dependence of V_{oc} on ln[I_3^-]. From the ratio of the slopes of the V_{oc} vs ln[I_3^-] (Figure 6) and V_{oc} vs ln P_0 (Figure 5a) plots, eq 10 yields a value of $m = 1.9$, implying that the reaction rate for recombination is second order in I_3^-. This result is consistent with transient absorption studies of I^- ions in colloidal TiO_2 solution.[34,35] The second-order process is attributed[34,35] to dismutation of I_2^- to I_3^- and I^-. An analogous reaction occurs in particulate systems containing Br^- ions.[36] Taking the dismutation reaction into consideration, the mechanism for back electron transfer is described as follows:

$$I_3^- \rightleftharpoons I^- + I_2 \tag{20}$$

$$e^- + I_2 \rightarrow I_2^- \tag{21}$$

$$2I_2^- \xrightarrow{\text{slow}} I_3^- + I^- \tag{22}$$

$$\text{net:} \quad 2e^- + I_3^- \rightarrow 3I^- \tag{1}$$

The chemical equilibrium (eq 20) and the reduction of I_2 (eq 21) are expected to play a prominent role in the overall reduction of I_3^- (eq 1).[37−39] Assuming the steady-state approximation and that the dismutation (eq 22) is rate limiting, the above mechanism yields a rate for recombination that is second order in I_3^- concentration. Furthermore, the presence of dismutation suggests that back electron transfer from TiO_2 involves I_2 as an electron acceptor. It is important to point out, however, that a different mechanism, not involving the dismutation of I_2^-, accounts for the reduction of I_3^- at the Pt cathode.[37,38]

Figure 5b shows that the I_3^- concentration has a significant effect on the variation of J_{sc} as a function of radiant power. At high I_3^- concentrations (>10 mM), J_{sc} of the untreated dye-covered electrodes exhibit a linear dependence on the radiant power up to 100 mW/cm^2 (15 ± 0.5 mA/cm^2; inset of Figure 5b), indicating no mass-transport limitation. In contrast, at low I_3^- concentration (2 mM), J_{sc} increases linearly with radiant power only at low radiant power (<10 mW/cm^2). At higher illumination levels, J_{sc} increases nonlinearly and tends toward saturation. The leveling off of J_{sc} with increasing radiant power can be attributed to a mass-transport-limited photocurrent, resulting from the depletion of I_3^- concentration at the Pt cathode. The I_3^- concentration at the Pt cathode is affected by the concentration gradient of I_3^- across the cell and therefore by the magnitude of the diffusion coefficient of the triiodide ions. The lowering of the I_3^- concentration at the Pt cathode at high photocurrent densities shifts the redox potential of I_3^-/I^- negatively, which increases J_r (eq 19) and leads to the nonlinear dependence of J_{sc} on the radiant power. The theoretical curve (solid line in Figure 5b) is generated with eq 19, using a nonlinear curve-fitting procedure. The calculated curve coincides closely with the experimental data for an optimized diffusion coefficient of 7.55×10^{-6} cm^2/s for I_3^- ions in CH_3CN/NMO (50:50 wt %)/TiO_2. After correcting for the TiO_2 porosity (0.3),[29] the diffusion coefficient of I_3^- ions in the solution phase is determined to be 2.5×10^{-5} cm^2/s, which is in good agreement with values obtained for I_3^- ions in CH_3CN [$(8.5-30) \times 10^{-6}$ cm^2/s] and NMO (2.8×10^{-6} cm^2/s).[37,38,40] The similarity of the calculated and measured values of the diffusion coefficient implies that I_3^- ions—and hence I_2—do not adsorb strongly to the TiO_2 surface and that their pathway through the porous TiO_2 film to the Pt cathode is not significantly longer than it would be in homogeneous solution. In other words, the porous structure of the TiO_2 films does not significantly retard the diffusion of I_3^- ions in the solution phase.

Figure 6 shows the dependence of V_{oc}, J_{sc}, FF, and η as a function of ln[I_3^-] for untreated dye-coated TiO_2 electrodes. Both J_{sc} and FF increase with ln[I_3^-], eventually leveling off at an I_3^- concentration larger than 10 mM. In contrast, V_{oc} decreases linearly with ln[I_3^-] for reasons discussed above. The poor FF (<0.6) at low I_3^- concentration (2 mM) is consistent with the depletion of I_3^- concentration at the Pt cathode. A low I_3^- concentration at the Pt cathode increases the overpotential for reduction (eq 1) at the electrode. The higher the overpotential, the poorer the fill factor—which determines the point of maximum power output—and the lower the conversion efficiency of the cell; a current-induced shift of the redox potential at the Pt cathode (eq 15) can also decrease FF. The variation of V_{oc}, J_{sc}, and FF with ln[I_3^-] determines an optimum conversion efficiency of 7% at an I_3^- concentration of 10 mM and a radiant power of 10 mW/cm^2.

In conclusion, the back electron transfer from dye-sensitized nanocrystalline TiO_2 films to the I_3^-/I^- couple in nonaqueous solution was studied. A potential drop at the SnO_2/TiO_2, interface, ohmic losses in SnO_2 and TiO_2, and an overpotential for the redox reaction at the Pt electrode cause a shift of potential and thus an apparent inequality between the dark current and recombination current at a specific voltage. Exposing the dye-coated TiO_2 electrodes to pyridine derivatives increases both the open-circuit photovoltage and conversion efficiency. An analytical expression describing the dependence of V_{oc} on interfacial recombination kinetics is derived, and its limitations are outlined. With the aid of this expression, the increase of V_{oc} correlates with a 1−2 order of magnitude decrease of the back-electron-transfer rate constant. Other phenomena (e.g., band edge displacement) may also, however, account for the effect of pyridine derivatives on V_{oc}. The rate of reaction for

back electron transfer is found to be second order, which is ascribed to the dismutation of I_2^- to I_3^- and I^-. At low I_3^- concentrations, the photocurrent becomes diffusion limited at high light intensities. Application of mass-transport theory to this situation yields a value for the diffusion coefficient of the triiodide ions through the nanoporous TiO_2 film.

Acknowledgment. We are grateful to Greg Smestad, Xiaoping Gao, and Sukumaran Muralidharan for their valuable comments. This work was supported by the Office of Basic Energy Sciences, Division of Chemical Sciences (G.S., A.J.N., and A.J.F.), and the Office of Utility Technologies, Division of Photovoltaics (S.Y.H.), U.S. Department of Energy, under Contract DE-AC36-83CH10093.

References and Notes

(1) Vlachopoulos, N.; Liska, P.; Augustynski, J.; Grätzel, M. *J. Am. Chem. Soc.* **1988**, *110*, 1216.
(2) Grätzel, M. *Coord. Chem. Rev.* **1991**, *111*, 167.
(3) O'Regan, B.; Grätzel, M. *Nature* **1991**, *353*, 737.
(4) Grätzel, M.; Liska, P. U.S. Patent 5 084 365, 1992.
(5) Kay, A.; Grätzel, M. *J. Phys. Chem.* **1993**, *97*, 6272.
(6) Nazeeruddin, M. K.; Kay, A.; Rodicio, I.; Humphry Backer, R.; Mueller, E.; Liska, P.; Vlachopoulos, N.; Grätzel, M. *J. Am. Chem. Soc.* **1993**, *115*, 6382.
(7) Grätzel, M.; Kalyanasundaram, K. *Curr. Sci.* **1994**, *66*, 706.
(8) Grätzel, M. *Platinum Met. Rev.* **1994**, *38*, 151.
(9) Grätzel, M. *Renewable Energy* **1994**, *5*, 118.
(10) Grätzel, M. *J. Sol-Gel Sci. Technol.* **1994**, *2*, 673.
(11) Mathews, D.; Kay, A.; Grätzel, M. *Aust. J. Chem.* **1994**, *47*, 1869.
(12) Grätzel, M.; Nazeeruddin, M. K. GB Patent 9 217 811, 1994.
(13) Saurer, E.; Grätzel, M.; Meyer, T. Fr. Patent 2 694 451, 1994.
(14) McEvoy, A. J.; Grätzel, M. *Sol. Energy Mater. Sol. Cells* **1994**, *32*, 221.
(15) Kavan, L.; Grätzel, M. *Electrochim. Acta* **1995**, *40*, 643.
(16) Grätzel, M. In *Research Opportunities in Photochemical Sciences*; DOE/BES Workshop Proc., Division of Chemical Sciences; Estes Park, CO; Feb 5−8, 1996.
(17) Knodler, R.; Sopka, J.; Harbach, F.; Grunling, H. W. *Sol. Energy Mater. Sol. Cells* **1993**, *30*, 277.
(18) Hagfeldt, A.; Didriksson, B.; Palmqvist, T.; Lindström, H.; Södergren, S.; Rensmo, H.; Lindquist, S.-E. *Sol. Energy Mater. Sol. Cells* **1994**, *31*, 481.
(19) Smestad, G.; Bignozzi, C.; Argazzi, R. *Sol. Energy Mater. Sol. Cells* **1994**, *32*, 259.
(20) Stanley, A.; Matthews, D. *Aust. J. Chem.* **1995**, *48*, 1294.
(21) Matthews, A.; Infelta, P.; Grätzel, M. *Aust. J. Chem.*, in press.
(22) Smestad, G. *Sol. Energy Mater. Sol. Cells* **1994**, *32*, 273.
(23) Liska, P. Ph.D. Thesis of Swiss Federal Institute of Technology, No. 1264, 1994.
(24) Hagfeldt, A.; Lindquist, S. E.; Grätzel, M. *Sol. Energy Mater. Sol. Cells* **1994**, *32*, 245.
(25) Hagfeldt, A.; Grätzel, M. *Chem. Rev.* **1995**, *95*, 49.
(26) Parkinson, B. A.; Furtak, T. E.; Canfield, D.; Kam, K.-K.; Kline, G. *Discuss. Faraday Soc.* **1980**, *70*, 233.
(27) The Butler−Volmer equation (Bard, A. J.; Faulkner, L. R. *Electrochemical Methods*; John Wiley and Sons: New York, 1980; p 103) has the form: $J = J_0[\exp(-\beta u\eta f) - \exp((1-\beta)u\eta f)]$. For the photopotential range studied ($\eta = V > 3kT/q = 80$ mV), the Butler−Volmer expression can be simplified by replacing the first exponential term with one. Furthermore, the resulting expression correctly predicts that when $J = 0$ mA/cm^2 (dark), $V = 0$ V. Substituting $-J = J_r$, $J_0 = qk_{et}c_{ox}^m n_0^{u\alpha}$, $\beta = 1 - \alpha$, $\eta = V$, and $f = q/kT$ into the simplified Butler−Volmer expression yields the equation $J_r = qk_{et}c_{ox}^m n_0^{u\alpha}[\exp(u\alpha qV/kT) - 1]$. Inserting eq 5 into this last expression gives eq 4.
(28) Kumar, A.; Sanatangelo, P. G.; Lewis, N. S. *J. Phys. Chem.* **1993**, *96*, 835.
(29) Papageorgiou, N.; Grätzel, M.; Infelta, P. P. *Sol. Energy Mater. Sol. Cells*, in press.
(30) Langmuir, M. E.; Parker, M. A.; Rauh, R. D. *J. Electrochem. Soc.* **1982**, *129*, 1705.
(31) *1993 Annual Book of ASTM Standards;* ASTM: Philadelphia, PA; Vol. 12.02, p E892.
(32) Fahrenbruch, A. L.; Bube, R. H. In *Fundamentals of Solar Cells*; Academic Press: New York, 1983; p 213.
(33) Eichberger, R.; Willig, F. *Chem. Phys.* **1990**, *141*, 159.
(34) Fitzmaurice, D. J.; Frei, H. *Langmuir* **1991**, *7*, 1129.
(35) Fitzmaurice, D. J.; Eschle, M.; Frei, H. *J. Phys. Chem.* **1993**, *97*, 3806.
(36) Frank, A. J.; Grätzel, M.; Kozak, J. J. *J. Am. Chem. Soc.* **1976**, *98*, 3317.
(37) Macagno, V. A.; Giordano, M. C.; Arvia, A. J. *Electrochim. Acta* **1969**, *14*, 335.
(38) Desideri, P. G.; Lepri, L.; Heimler, D. In *Encyclopedia of Electrochemistry of the Elements*; Bard, A. J., Ed.; Marcel Dekker: New York, 1973; Vol. 1, p 91.
(39) Gerischer, H.; Meyer, E. *Z. Phys. Chem. (Munich)* **1971**, *74*, 302.
(40) Papageorgiou, N.; Athanassov, Y.; Bonhôte, P.; Pettersson, H.; Grätzel, M. *J. Electrochem. Soc.*, in press.